Chapter 3

Random photo-illumination on segregating polymeric fluids

3.1 Introduction

Various stimuli like pressure, temperature, and chemical composition generally cause phase separation in polymeric fluids, including polymer blends, block copolymer (BCP) melts, and solutions [85,86]. The enhanced characteristics and functionality of the resulting materials have attracted significant interest in various industrial applications [69–73,105]. Over many decades, various soft materials like polymers and gels have garnered significant interest due to their enhanced properties when influenced by external stimuli such as light, leading to numerous applications [56,60,66,74,75,106]. Among the many applications of controlled polymerization techniques, photoinitiated controlled free radical polymerization (Photo-CRP) is particularly effective in producing responsive soft materials. These materials have diverse applications, including in biomaterials, coatings, adhesives, and self-healing systems [107–117]. For instance, a recent paper describes a visible light photo-CRP approach [60] that alters the composition and structure of

mother polymer gels, opening up new possibilities for light-induced modification of soft materials [56,56,60,74,75].

The phase separation kinetics of polymeric fluids under external photo-illumination has been a fascinating research field for a few years [47]. Photo-CRP initiates bond-breaking reactions that generate active radicals. These newly formed free radicals enable cross-linking and chain exchange reactions [56,60,74,75]. In contrast, radical termination and bond combination reactions are initiated when the light is off [118–120]. With this concept, we can modify the properties of soft materials by manipulating the size and morphology of distinct phases [47]. Comprehending the influence of light on the phase separation kinetics of polymeric fluids can open avenues for creating novel materials with altered characteristics applicable in areas such as wound healing, sensors, and microfluidics. This renders the research field exceedingly promising for the progression of material science [56,60,74,75].

In the preceding chapter (Chapter 2) [47,121], we explored the phase separation kinetics of a BCP melt system subjected to on/off-light cycles of equal durations. The BCP chains were assumed to possess photo-sensitive bonds linking the incompatible blocks. In this study, we employed the recently developed photo-CRP model with the DPD approach [56,57,60] to examine domain morphology, length scale, characterization functions, and reaction kinetics [25]. Based on previous experimental data, our model accurately replicated the CRP kinetics and gel formation [59,74,76,102]. The findings revealed that the first on-cycle primarily influenced the scaling behavior of the system. Following the first on-cycle, the kinetics adhered to the same universality class regardless of subsequent on-off-cycles [47]. In the early cycles, deviations in the scaling function were observed until the kinetics were controlled by bond-breaking reactions during the first on-cycle. During the on-cycles, the system undergoes macro-phase separation due to bond-breaking reactions [23,25]. In contrast, micro-phase separation occurs during off-

cycles due to bond-recombination reactions [63,67,95]. In our modeling approach, direct light utilization is not involved. Hence, this model can be utilized for a comprehensive exploration of bond-breaking reactions induced by any form of deformation within the system, such as stretching of the simulation box [66,101,122].

In the current chapter, we investigate the influence of random photo illumination on the phase separation kinetics of polymer fluids. We examine two distinct systems: (i) A critical binary polymer blend with active radicals located at one end of each polymer chain. (ii) A symmetric BCP melt with photo-sensitive bonds joining the two incompatible blocks. In the off-state of light [57,60], the active radicals within the polymer chains undergo bond recombination reactions, while the photo-sensitive bonds undergo bond-breaking reactions when the light is in on-state [47,56,57,60]. Initially, we equilibrate the system at a high temperature to achieve an uncorrelated state. Subsequently, we perform a temperature quench below the miscibility gap, inducing phase separation in the system. Concurrently, we apply random photo-illumination to study its effect on the phase separation kinetics of polymer fluids [23,25]. Further details are discussed in following sections.

3.2 Modeling random photo-illumination

We applied random photo-illumination to the system, where the light's on-state breaks the photo-sensitive bonds in the BCP chains, generating two active radicals of incompatible beads. These active radicals undergo bond-recombination reactions in the light's off-state [56,57,60]. The corresponding schematic diagram is illustrated in Fig. 3.1. The mechanism of bond-breaking and bond-recombination reactions are already discussed in chapter 2, section 2.2. Other reactions, such as coupling of the same radicals and chain transfer polymerization, are neglected in the present study as they may hinder the bond-recombination reaction between the two BCP blocks [47,56,57,60]. The probabilities

of bond-breaking and recombination reactions are denoted as P_b and P_c, respectively. Based on prior DPD studies, the reaction time step is fixed at $\tau_r = 10\Delta t$ [47,56,57,60,66].

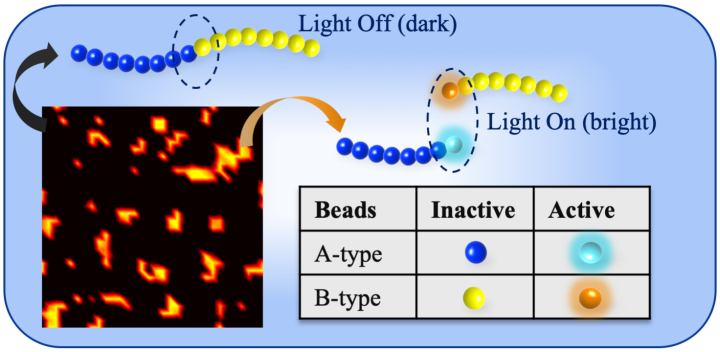

Fig. 3.1: Schematic of bond-breaking and combination reactions under random photo-illumination. The inactive A and B-type beads are represented by blue and yellow. At the same time, the corresponding active radicals are shown with glowing cyan and glowing orange.

In the previous chapter, we showed that the fraction of bond-broken n_b over time follows first-order reaction kinetics of bond degradation [47,66]. At a fixed P_b, we determined that $n_b(t) \simeq [1 - \exp(-kt)]$, with $k = P_b/\tau_r$ as the rate constant. The rate constants have values $k = 0.01$, 0.05, and 0.1 for $P_b = 0.1$, 0.5, and 1.0, respectively. Prior research [122–125] indicates that the bond-breaking rate constants have values within the range from 1.0 to $10^{-3}s^{-1}$ for various polymer systems undergoing photo-controlled degradation. This suggests that the bond-breaking reactions occur significantly slower than the characteristic diffusion times at relevant length scales [47,66], ensuring that our system operates within a kinetically controlled regime.

3.3 System details

In our study, we have examined two systems. The first is a critical binary polymer blend system with polymer chains A_n and B_n, where $n = 16$. Each polymer chain has one active radical at one end. The second system is a BCP melt, with each polymer chain consisting of two linear incompatible blocks, A_n and B_n, where $n = 16$. The bond joining

the two blocks is considered photosensitive. We used a cubic simulation box with a size of $L = 64$ and periodic boundary conditions in all three directions. The system density is $\rho = 3$, resulting in $N = \rho \times L^3 = 7,86,432$ DPD beads. Therefore, the total number of polymer chains in the binary polymer blend is $n_p = N/n = 49,152$, and in the BCP melt, it is $n_p = 24,576$. As discussed earlier, varying the bond-breaking probability P_b simulates changes in light intensity. We varied $P_b \in (0, 1)$ throughout our simulation study while keeping the bond recombination probability fixed at $P_c = 1.0$. Our research focuses on general polymer systems exposed to random photo illumination.

First, we considered the system at a high temperature ($T = 10$) and equilibrated it for an extended period up to $t = 2 \times 10^3$ to achieve a uniformly mixed state. Subsequently, we quenched the system below the critical temperature $T = 1$, reset the time $t = 0$, and studied the photo reaction kinetics, scaling, and growth laws. Simultaneously, we applied random photo-illumination to the system to investigate its effect on the phase separation kinetics of polymer fluids.

3.4 Polymer blend system

3.4.1 Domain morphology and reaction kinetics

We fixed the bond recombination probability $P_c = 1$ and varied the bond breaking probability $P_b \in (0.1)$. For four different values of $P_b = 0.01$, 0.1, 0.5, and 1.0, we have plotted the evolution snapshots in Figs. 3.2(a)-3.2(d). The A and B-type beads are represented by blue and yellow colors, respectively. As P_c is set to its maximum value, the lowest bond-breaking probability results in the maximum number of bond recombination reactions between the unfavorable active radicals while bond-breaking remains minimal. Consequently, the polymer blend system behaves like block copolymer melt, resulting in microphase separation over time (see Fig. 3.2(a)). In contrast, at higher P_b values, the

bond-breaking reactions cause a significant number of photo-sensitive bonds to break. The system then behaves as a polymer blend, leading to macrophase separation via spinodal decomposition (see Fig. 3.2(d)). Hence Figs. 3.2(a)-3.2(d) show that with the increase of P_b, the kinetics shift from the microphase separation of the BCP melt ($P_b = 0$), to the macrophase separation in the polymer blend ($P_b = 1$) [47].

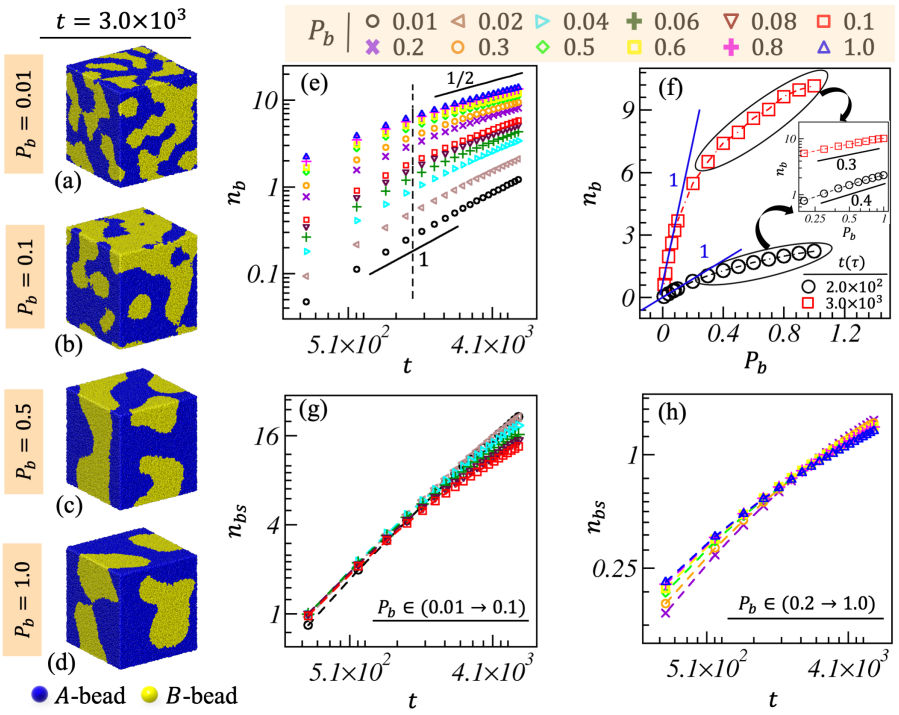

Fig. 3.2: (a-d) Domain evolution snapshots of polymer blend system for different bond breaking probabilities at $t = 3.0 \times 10^3$. Blue and yellow colors represent A and B beads, respectively. (e) Time variation of the normalized cumulative number of bonds broken (n_b) at various P_b values. (f) n_b vs. P_b at two different time intervals $t = 2.0 \times 10^2$ and 3.0×10^3 plotted with black and red curves, respectively. Inset plots the n_b vs P_b on log-log scale at higher P_b values. (g) Scaling of the normalized cumulative number of bonds broken at low P_b values $(0.01 - 0.1)$. Corresponding scaled data is denoted as n_{bs}. The scaling at higher P_b values $(0.2 - 1.0)$ is shown in (h). Legends at the top represent the different P_b values depicted with various symbol types.

Suppose we have applied only off-light state to the polymer blend system; it can form the maximum number of $N_{pc} = 24,576$ light-sensitive bonds [47,66]. In our study, bond-breaking and reformation reactions co-occur in the system due to random photo illumination. We calculate the cumulative number of bonds broken over time and

normalize it by N_{pc}. The corresponding normalized cumulative number of broken bonds n_b vs. t is plotted in Fig. 3.2(e) on a logarithmic scale for different P_b values, as indicated in the legend with various symbols. Following fitting, we observe a power law growth in each plot: $n_b \sim t^{\theta}$ for all bond-breaking probabilities. Here, θ represents the growth exponent. Until reaching a crossover time, $t_r \sim 1.3 \times 10^3$, θ remains constant across all P_b values, with a value of unity. Beyond the specified crossover time, the growth exponent decreases as P_b increases. At $P_b = 0.01$, the exponent approximates $\theta \sim 1$, whereas at $P_b = 1.0$, it approximates $\theta \sim 0.5$. This observation aligns with the trend of the solid black line, which exhibits slopes of 1 and 1/2, respectively, confirming the same conclusion. In Fig. 3.2(f), the n_b vs. P_b curve is plotted at two different time intervals: $t = 2.0 \times 10^2$ (black curve) and $t = 3.0 \times 10^3$ (red curve). These curves also exhibit a power law behavior, $n_b \sim {P_b}^{\theta}$. For smaller P_b values, ranging from 0.0 to 0.2 in the black curve and 0.0 to 0.06 in the red curve, θ maintains a value of 1, indicating linear growth. However, at higher probabilities, the growth exponent decreases. The inset shows that as P_b approaches 1.0, the growth exponent takes on 0.4 and 0.3 values in the black and red curves, respectively.

Based on the results depicted in Fig. 3.2(f), we further analyze the n_b vs. t plots presented in Fig. 3.2(e). We observe two distinct scaling behaviors. In Fig. 3.2(g), a noticeable overlap of data at early time intervals indicates that the plots for n_b over time follows a linear behavior for all P_b values. However, at later times, a significant deviation is observed as $P_b \to 1.0$. Consequently, we have plotted the data only for $P_b \in (0.01, 0.1)$ and omitted the remaining for clarity. For higher P_b values within the range of $(0.2, 1.0)$, we observe a significant scaling in the data with a power law equation having lower exponents, as illustrated in Fig. 3.2(h). Although some deviation is noticed at early times, an excellent collapse is observed later on. Overall, at low bond-breaking probabilities, only a limited number of bond-breaking reactions are occurring in the

system. Consequently, n_b vs. t follows a power law behavior with $\theta = 1.0$. However, at higher probability values, the growth exponent decreases due to the occurrence of a sufficient number of bond-breaking reactions.

3.4.2 Radial distribution function

To quantify the domain evolution, we plotted the RDF in Fig. 3.3(a) at different time intervals with a fixed $P_b = 0.5$. As time increases, the prominent peak of the RDF curves shifts towards higher r values. For example, the peak shifts from $r = 16.0$ (black) to $r = 28.16$ (blue) over time. We estimate the average distance between the particles by examining the position and height of the primary peak. The shifting of peaks towards higher r values signifies the growth of the domains over time.

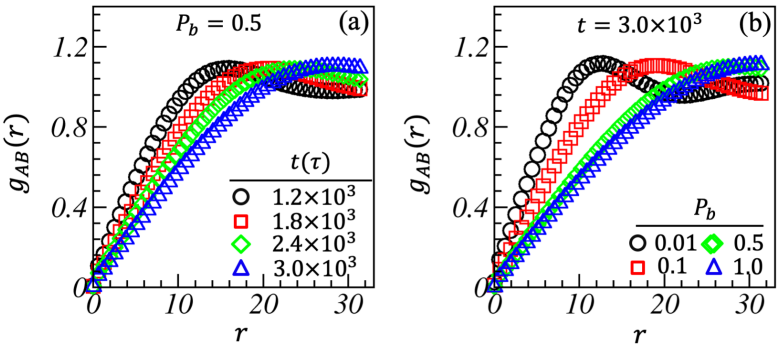

Fig. 3.3: (a) Radial distribution function, $g_{AB}(r)$, at $P_b = 0.5$. Different symbol types in the legends represent different time intervals. (b) Comparison of $g_{AB}(r)$ vs, r at different P_b values at a late time $t = 3.0 \times 10^3$.

Corresponding to the evolution shown in Figs. 3.2(a)-3.2(d), we plot $g_{AB}(r)$ vs. r in Fig. 3.3(b) at $t = 3.0 \times 10^3$ for different P_b values given in the legends as $P_b = 0.01, 0.1, 0.5$, and 1.0. We notice the broadening in primary peaks at higher P_b values. At the same time, the RDF peaks are shifting towards higher r values as: $r = 12.8, 19.2, 28.16$, and 31.36 in the black, red, green, and blue curves, respectively. At a very small value of $P_b = 0.01$, the formation of microdomains can be observed through the appearance of a secondary peak in the black curve, starting at $r = 22.4$. However, at higher P_b

values, the secondary peaks disappear from the RDF curves, indicating the formation of a macrophase-separated structure. These findings demonstrate the increased growth of the domains at higher bond-breaking probabilities.

3.4.3 Characterization functions and anisotropy

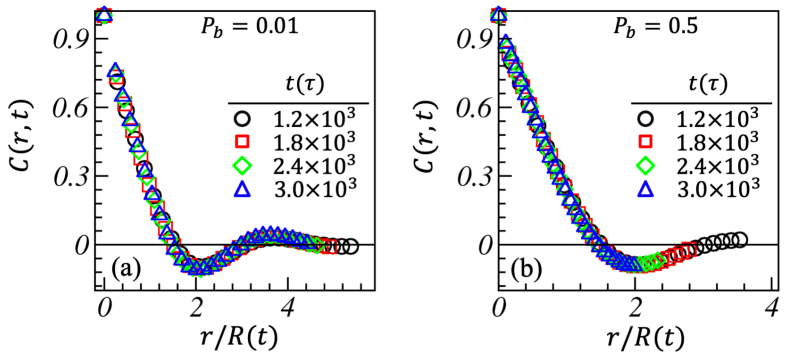

Fig. 3.4: Spherically averaged scaled correlation function $C(r,t)$ vs. $r/R(t)$ at different time intervals are plotted with different symbols at $P_b = 0.01$ in (a) and $P_b = 0.5$ in (b). The solid black line represents the zero-crossing.

In Fig. 3.4, we plot the spherically averaged correlation function $C(r,t)$ against $r/R(t)$ for different time intervals at two different P_b values: $P_b = 0.01$ (Fig. 3.4(a)) and $P_b = 0.5$ (Fig. 3.4(b)). For fixed light intensities, the good overlap in the scaling function curves indicates that the evolved morphologies belong to the same universality class under random photo illumination. The zero crossing of the correlation function is highlighted with a solid black line. At both probabilities, the oscillations of the correlation curves diminish over time, and the tails of the $C(r,t)$ curves shift towards lower r values, indicating domain growth in the system. At higher light intensity, the shifting of tails towards lower r values is more pronounced due to the increased growth rate. This can be understood through the basic concept of a binary fluid system with two phases separated by a boundary; the composition density is conserved. At the interfaces, the composition changes, resulting in a gradient in the order parameter and local density. The correlation function measures the relationship between the densities at different

points (e.g., $\vec{r}_1$ and $\vec{r}_2$). Due to the constraint of composition conservation, the sum rule $\int C(\vec{r},t)d\vec{r} = 0$ is enforced, where $\vec{r} = \vec{r}_1 - \vec{r}_2$. Consequently, it oscillates when the correlation function encounters the interfaces between the two phases. As time advances, the domain size increases, leading to a reduction in the number of interfaces. Thus, the oscillatory behavior of the correlation curves diminishes over time. Continuing, the oscillations in the curves disappear after a much longer time when the domain sizes are roughly equal to the system size. However, some correlation remains due to the presence of well-defined large domains of the two components.

To examine the effect of different light intensities, we compared the scaled correlation function $C(r,t)$ vs. $r/R(t)$ at various P_b values: $P_b = 0.01$, 0.1, 0.5, and 1.0, represented by black, red, green, and blue curves, respectively. The data is compared for two different time intervals: Fig. 3.5(a) at an early time $t = 1.2 \times 10^3$ and Fig. 3.5(b) at a later time $t = 3.0 \times 10^3$. At both time intervals, for the lower P_b value of 0.01, the oscillatory nature of the correlation curve indicates the development of periodic morphology, as seen in the black curve. The oscillations decrease with an increase in P_b up to 0.1, as shown by the red curve. As discussed earlier, with the increase in the rate of bond-breaking reactions, the system behaves like a polymer blend, resulting in macrophase separation over time. Consequently, in the green ($P_b = 0.5$) and blue ($P_b = 1.0$) curves, the correlation function terminates at shorter distances, specifically $r/R(t) = 3.53$ and 3.19 in Fig. 3.5(a) and $r/R(t) = 1.99$ and 1.76 in Fig. 3.5(b). An excellent overlap in data is noted at higher probabilities, except for a small deviation at $P_b = 0.01$. This indicates that the corresponding morphologies for the given time steps are equivalent. However, at the later time intervals, their statistical properties are independent of the higher light intensities and thus belong to the same universality class.

In Figs. 3.5(c) and 3.5(d), we plot the unidirectional structure factor $S(k_x, k_y, k_z)$ against k_x, k_y, and k_z to demonstrate the anisotropy developed in the system. The

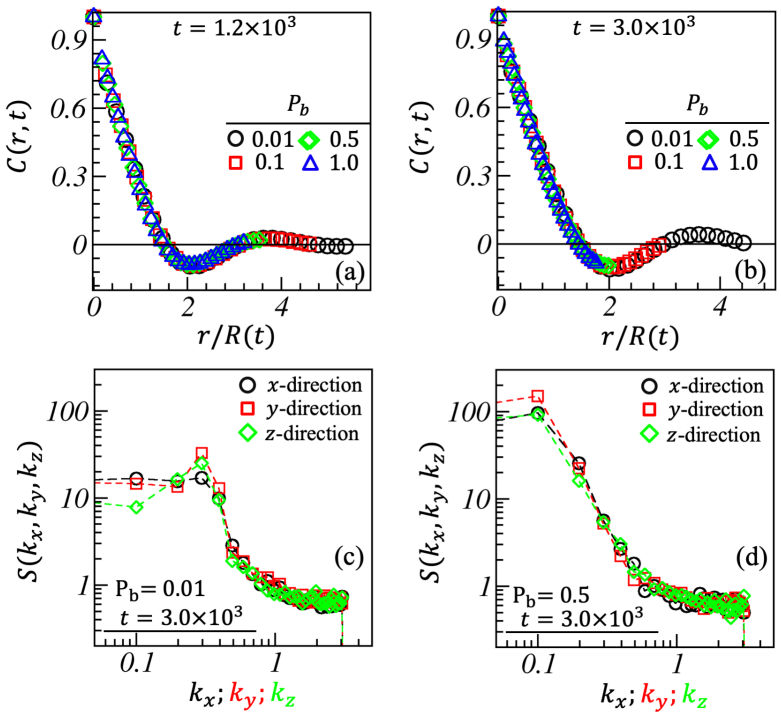

Fig. 3.5: (a-b) Scaled correlation function $C(r,t)$ vs. $r/R(t)$ for different bond-breaking probability $P_b = 0.01$, 0.1, 0.5, and 1.0 plotted with black, red, green, and blue curves respectively for $t = 1.2 \times 10^3$ in (a), and $t = 3.0 \times 10^3$ in (b). Corresponding evolved morphologies are displayed in Figs. 3.2(a)-3.2(d). (c-d) Plots for the structure factor along x, y, and z direction at $t = 3.0 \times 10^3$ are displayed in (c) for $P_b = 0.01$ and (d) for $P_b = 0.5$ to discuss the anisotropy developed within the system.

structure factor data is shown at the later time $t = 3.0 \times 10^3$ for $P_b = 0.01$ in (c) and $P_b = 0.5$ in (d). At this later time, the anisotropy in the system is evident in the non-overlapping curves along all three directions. The structural anisotropy is more pronounced at $P_b = 0.01$, where the system exhibits BCP melt behavior. Here, the data is plotted only for two given P_b values. However, at higher bond-breaking probabilities, the structure factor along different directions shows excellent overlap, indicating isotropic domains.

3.4.4 Growth laws

With varying the bond breaking probability, we have calculated the characteristic domain length $R(t)$ over time plotted in Fig. 3.6(a). At a fixed P_c, the change in P_b works as a control parameter for the domain coarsening under random photo illumination. As P_c is set to its maximum value, at a lower bond-breaking probability the free radicals undergo rapid bond-recombination reactions. Consequently, very few bond-breaking reactions occur, causing the system to effectively behave like a BCP melt. As a result, at lower probability: $P_b \in (0.005, 0.1)$ the characteristic length follows the usual diffusive growth ($\phi \sim 1/3$) within the early spinodal time window up to $t_{sp} \sim 6.0 \times 10^2$. For a reference case, we have plotted the length scale of pure BCP melt and pure polymer blend systems with black and magenta dashed lines, respectively. At minimal P_b values, specifically, $P_b = 0.005$ and 0.01 denoted by the violet and black symbols, the length scale follows the pure BCP melt behavior, showing the diffusive growth in early times and crosses over to saturation later. In these cases, the growth rate is higher than that of the BCP melt system because of early macroscopic growth. For $P_b \in (0.015, 0.1)$, we observe a deceleration in growth within a limited time frame (also visible in Fig. 3.6(c)), which later transitions to faster growth.

On further increase in P_b, the macrophase separation starts dominating over the BCP melt behavior, leading to increased growth than usual diffusive growth ($\phi \sim 1/3$) during the initial times. In a pure binary polymer blend, the early-time diffusive growth is very short-lived in the length and time scale of DPD simulations [47], and the viscous hydrodynamic growth ($\phi \sim 1$) is typically observed. In our study, bond-breaking and bond-recombination reactions occur simultaneously. A higher value of P_b accelerates coarsening, while the fixed maximum value of P_c decelerates it in the background. This interplay of reaction kinetics results in a growth exponent $1/3 < \phi < 1$ at early times. With a further increase in P_b, the length scale eventually transitions to the inertial

hydrodynamic growth regime ($\phi \sim 2/3$) at late times. Comparing the length scale with the pure BCP melt and pure polymer blend system, it can be concluded that the increased intensity of illuminated light leads to the transition from micro- to macro-phase separation kinetics. As $P_b \to 1.0$, the system exhibits behavior of a binary polymer blend at late time intervals.

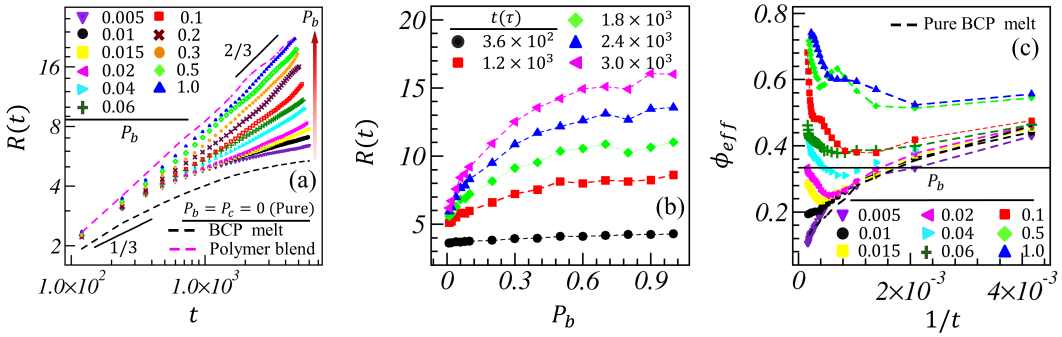

Fig. 3.6: (a) The characteristic length scale $R(t)$ vs. t for different bond-breaking probabilities $P_b \in (0.0, 1.0)$ at a fixed bond recombination probability $P_c = 1.0$. The solid lines represent the growth laws followed by the system (1/3 for the diffusive growth and 2/3 for the inertial hydrodynamic growth). For a reference case, the length scale of pure BCP melt and pure polymer blend is plotted with the black and magenta curves. (b) Plots for $R(t)$ vs. P_b at different time intervals are depicted with various symbol types in the legends. (c) ϕ_{eff} vs. $1/t$ for different bond-breaking probabilities plotted with various symbols given in the legends.

We further analyze the data for the length scale by plotting $R(t)$ vs. P_b at different time intervals in Fig. 3.6(b). After fitting, we observe a power law behavior $R(t) \sim P_b^{\nu}$ for each curve, where ν is the power law exponent. For the given time intervals $t = 3.6 \times 10^2$, 1.2×10^3, 1.8×10^3, 2.4×10^3, and 3.0×10^3, the power law exponents have values $\nu = 0.03$, 0.13, 0.17, 0.2, and 0.23, respectively. Next, we have plotted the effective growth exponent ϕ_{eff} against $1/t$ in Fig. 3.6(c) for different P_b values, as mentioned in the legend. As discussed earlier, the violet and black curves plotted for $P_b = 0.005$ and 0.01 show a decreament in the growth exponent, which later tends zero in assymptotic limit. These curves represent the BCP melt behavior (indicated by the black dashed line) followed by the system at lower P_b values. At higher values of P_b, ϕ_{eff} increases,

particularly at later times, as discussed in Fig. 3.6(a). At much higher photo intensity values ($P_b \to 1.0$), the system follows the inertial hydrodynamic regime during the later time intervals. When comparing their late-time behavior, all curves at higher P_b values approach the inertial hydrodynamic regime in the asymptotic limit.

We initialized the simulation with a polymer blend system at the time of temperature quench, so the natural behavior of the system is macrophase separation. However, as time progresses, the effect of bond recombination reactions at $P_c = 1.0$ (which cause microphase separation) begins to dominate the phase separation kinetics for $P_b > 0.015$, resulting in the creation of reasonably sized microphase-separated domains. At that point, there is a competition between micro- and macro-phase separation kinetics. Consequently, for $P_b > 0.015$, macrophase separation is slowed down at early times. However, over time, the system revives the effect of bond recombination reactions and eventually transitions to macro-scale growth. This significant point indicates that $P_b \simeq 0.015$ can be considered the transition probability from micro- to macro-phase separation kinetics.

3.5 BCP melt system

In this analysis, we consider a system initially consisting of a block copolymer (BCP) melt with light-sensitive bonds between incompatible blocks of types A and B. As in the previous case, the system is subjected to photo-illumination in a random fashion with $P_c = 1.0$. The bond-breaking probability has values $P_b \in (0, 1)$ and mimics the change in the intensity of photo-illumination. In a BCP chain, two active radicals of different types are generated on the bond-degradation reaction. During the off-light cycle, the active radicals undergo the bond-recombination reaction, reforming the original BCP chains. We randomly applied the light to the system and investigated its effect on the phase separation kinetics of the BCP melt system. As the BCP melt's kinetics is very slow

compared to the macrophase separation kinetics of the polymer blend, we have simulated the present system for an extended period $t = 1.2 \times 10^4$.

3.5.1 Domain morphology and reaction kinetics

For four different values of P_b $(0.01, 0.1, 0.5,$ and $1.0)$, we have plotted the evolution snapshots at the late time $t = 1.2 \times 10^4$ in Figs. 3.7(a)-3.7(d). The blue and yellow colors in these snapshots represent A and B type beads, respectively. The evolution of the morphology indicates that as the bond-breaking probability increases, the degree of coarsening also increases. At higher rates of bond-breaking reactions, more photo-sensitive bonds are broken, accelerating the domain coarsening process.

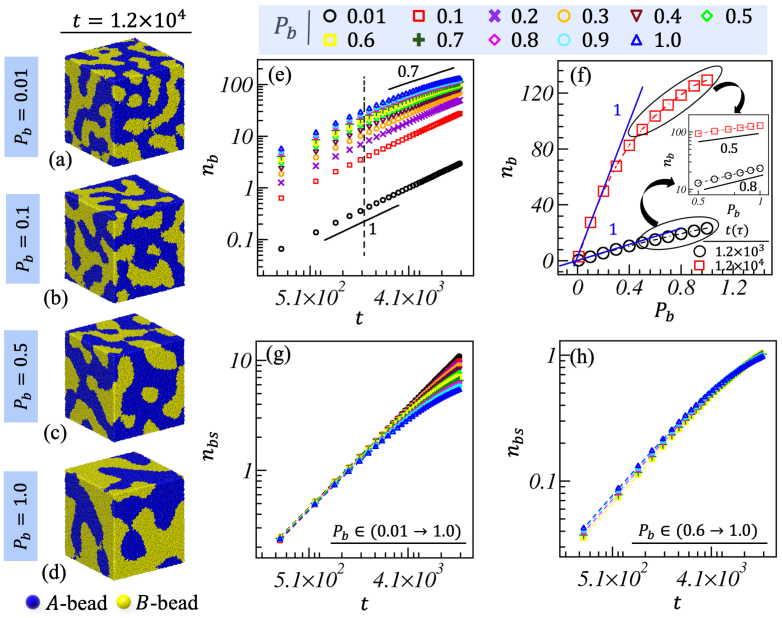

Fig. 3.7: (a-d) Domain evolution of BCP melt system at different light intensities: $(P_b = 0.01, 0.1, 0.5,$ and $1.0)$ at $t = 1.2 \times 10^4$. (e) Time-dependent behavior of n_b at different bond-breaking probabilities. (f) n_b vs. P_b at two different time intervalas: $t = 1.2 \times 10^3$ (black curve) and $t = 1.2 \times 10^4$ (red curve). Inset plots the data at high P_b values representing the power law growth. (g) and (h) plot the n_b vs. t data after scaling with the power law equation with the unit and lower growth exponents, respectively.

In Fig. 3.7(e), we have plotted the time variation of n_b for different values of P_b, indicated by various symbols in the legend. Here, n_b represents the cumulative number

of broken bonds normalized by N_{pc}, where $N_{pc} = 24,576$ is the maximum number of photo-sensitive bonds present in the system at $t = 0$. As time progresses, n_b increases due to the occurrence of bond-breaking and bond-recombination reactions. Similar to the polymer blend system, n_b vs. t follows a power law behavior: $n_b \sim at^\theta$, where θ is the growth exponent. A vertical dashed line in the plot represents a transition time $t_r \simeq 1.3 \times 10^3$. For $t < t_r$, the growth exponent θ is 1.0 for all P_b values. At later time intervals beyond t_r, the growth exponent decreases. For $P_b \lesssim 0.2$, the growth exponent remains approximately $\theta \simeq 1$, while for $P_b = 1.0$, it reduces to $\theta \simeq 0.7$. Two solid lines characterize the late-time behavior of the data: one with a slope of 1.0 for lower P_b values, which decreases to a slope of 0.7 as P_b approaches 1.0.

At a fixed $P_c = 1.0$, we vary P_b within the range (0.0, 1.0). In Fig. 3.7(f), we plot n_b vs. P_b at two different time intervals: $t = 1.2 \times 10^3$ (black curve) and $t = 1.2 \times 10^4$ (red curve). In both time intervals, n_b exhibits a power law dependence on P_b, as discussed in the previous case of the polymer blend system. At lower bond-breaking reaction probabilities ($P_b < 0.4$), the growth exponent is $\theta = 1.0$ and decreases with increasing P_b. To estimate the growth exponent at higher probabilities, we plotted the n_b vs. P_b data on a log-log scale in the inset of Fig. 3.7(f). From these plots, we obtained $\theta = 0.8$ at early times and $\theta = 0.5$ later. The increase in P_b influences the number of bond-breaking and bond-recombination reactions. Consequently, the growth exponent decreases at higher P_b values.

Based on the behavior of the curves in Fig. 3.7(f), we scale the n_b vs. t plots in Figs. 3.7(g)-3.7(h). We denote the scaled data of n_b as n_{bs}. In Fig. 3.7(g), we notice a good overlap in the data for $P_b < 0.4$, indicating the linear growth of n_b over time. However, deviations from the linear behavior are noted at later time intervals and higher probabilities. In Fig. 3.7(h), we have scaled the data using a power law equation with a lower growth exponent, less than one. An excellent scaling is observed for $P_b > 0.4$,

indicating the power law behavior at higher probabilities and later times. It is worth noting that we observed similar behavior of n_b over time for different P_b in the case of the polymer blend system. Thus, the impact of light exposure on the reaction kinetics of both systems is qualitatively the same.

3.5.2 Characterization functions

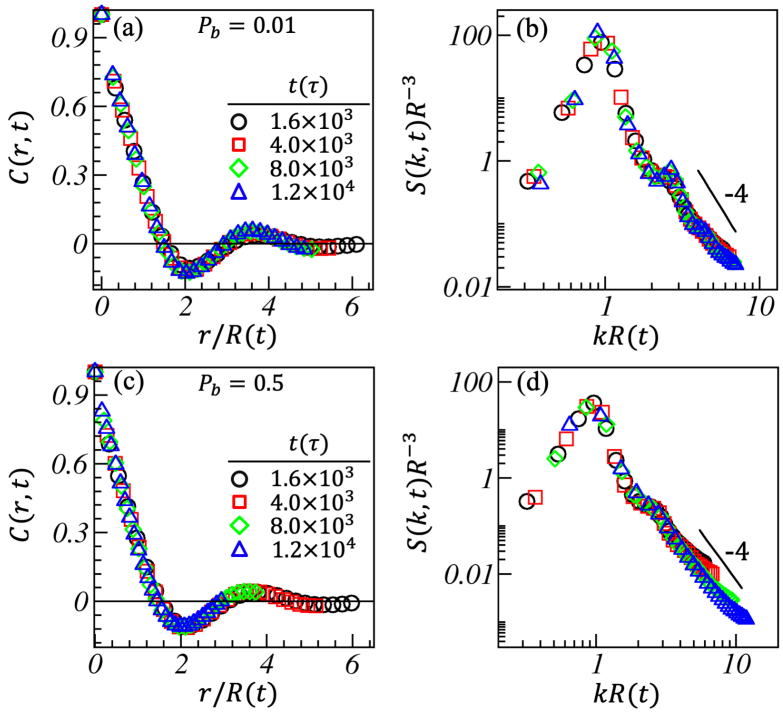

Fig. 3.8: (a-b) Comparison of the scaled correlation function and structure factor for $P_b = 0.01$ at various time intervals, depicted by different symbols. In (a), $C(r,t)$ vs. $r/R(t)$ curves are plotted on a linear scale, while (b) shows $S(k,t)$ vs. $kR(t)$ on a logarithmic scale. (c-d) The same quantities are plotted for $P_b = 0.5$.

To characterize the evolution of morphology at different time intervals, we have plotted the spherically averaged scaled correlation function $C(r,t)$ vs. $r/R(t)$ and the corresponding structure factor $R^{-3}S(k,t)$ vs. $kR(t)$ in Fig. 3.8. In Figs. 3.8(a)-3.8(b), we present the scaling functions for $P_b = 0.01$, while Figs. 3.8(c)-3.8(d) display the same data for $P_b = 0.5$. The legends indicate the time steps, represented by various symbols.

In Figs. 3.8(a) and 3.8(b), the excellent overlap in the scaling function data indicates a statistically self-similar morphology at different time intervals, suggesting they belong to the same universality class. As time progresses, the correlation function terminates at shorter distances, indicating the formation of larger clusters over time. At lower $P_b = 0.01$ (Fig. 3.8(a)), the system behaves effectively like a BCP melt due to the low rate of bond-breaking reactions, leading to slow domain growth. Consequently, the change in $C(r,t)$ is smaller in Fig. 3.8(a) compared to Fig. 3.8(c). In the structure factor plots, we observe sharper first peaks and a distinct shoulder in Fig. 3.8(b) ($P_b = 0.01$). This indicates the formation of more periodic microstructures, such as an incipient lamellar structure, compared to Fig. 3.8(d) at higher $P_b = 0.5$. However, the solid black lines with a slope of -4 in Figs. 3.8(b) and 3.8(d) represent Porod's law, $S(k,t) \sim k^{-4}$, followed by the tails of the structure factor curves for $k \to \infty$ [27].

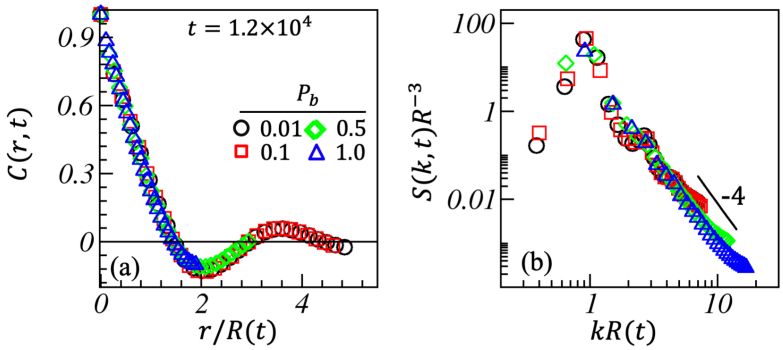

Fig. 3.9: (a-b) Comparison of the correlation and the structure factor curves for different bond-breaking probabilities P_b: 0.01 (black), 0.1 (red), 0.5 (green), and 1.0 (blue), at a late-time regime, $t = 1.2 \times 10^4$.

Next, we compare the scaling function data at a late time interval ($t = 1.2 \times 10^4$) for various P_b values indicated in the legends. We plot $C(r,t)$ vs. $r/R(t)$ in Fig. 3.9(a) and $R^{-3}S(k,t)$ vs. $kR(t)$ in Fig. 3.9(b). We observe a good overlap in the scaling function data for each P_b, except for a slight deviation noted at lower probabilities. At lower bond-breaking probabilities ($P_b = 0.01$ and 0.1), the appearance of a distinct shoulder indicates the formation of an incipient lamellar structure resulting from microphase

separation kinetics. However, at higher P_b values, the distinct shoulder vanishes from the structure factor due to the occurrence of macrophase separation kinetics. The scaled structure factor curves consistently follow Porod's law ($S(k,t) \sim k^{-(d+1)}$) at all times. Here, d represents the dimensionality of the system.

3.5.3 Growth laws

In Fig. 3.10(a), we plot the characteristic length scale over time for different light intensities. The solid black lines with slopes 1/3 and 2/3 represent the growth laws followed by the system during evolution. For comparison with the behavior of the system during microphase evolution, we have plotted the length scale for a pure BCP melt system as a reference case, shown by the black dashed curve. At early times, up to the spinodal time window $t_{sp} \sim 1.0 \times 10^3$, the system exhibits diffusive growth $R(t) \sim t^{1/3}$ for all P_b values. This behavior aligns with any BCP melt system at early times, representing the occurrence of microphase separation via spinodal decomposition. During this spinodal time window, all curves coincide with $R(t_{sp}) \sim 4.0$. This observation suggests that regardless of the light intensities, the domain coarsening initiates with spinodal decomposition, following the microphase separation kinetics consistent with typical behavior seen in BCP fluids. Since we began with the BCP melt, the system exhibits typical microphase separation behavior, resulting in fewer bond breakages within the system at early times. Consequently, the value of t_{sp} is much higher in BCP melt compared to the previous case of polymer blend systems ($t_{sp} \sim 6.0 \times 10^2$).

The impact of photo-illumination on the bond constraint in the BCP chains becomes apparent for $t > t_{sp}$. At lower rates of bond-breaking reactions ($P_b < 0.2$), microphase separation dominates over the effect of external light. Consequently, the curves plotted with cyan, red, and purple symbols crossover to saturation at later times. For $P_b > 0.2$, the slope of the length scale initially decreases but eventually crosses over to faster growth.

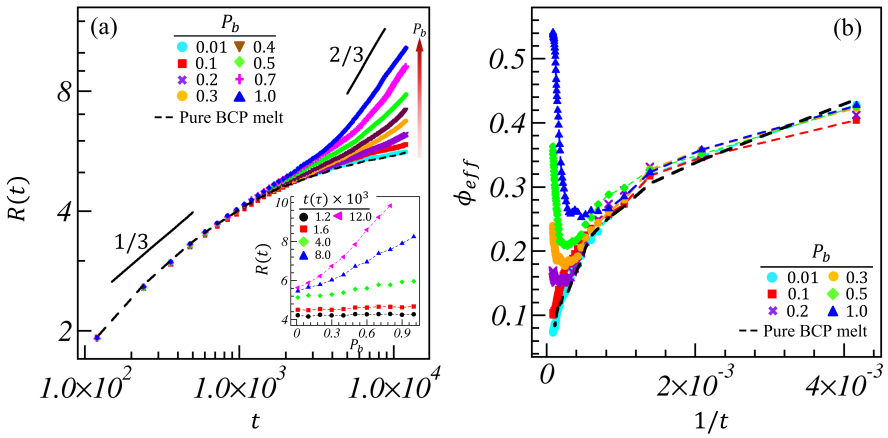

Fig. 3.10: (a) The characteristic domain size, $R(t)$ vs. t on a logarithmic scale for various P_b values. The length scale for a pure BCP melt system is plotted with a black dashed curve for a reference case. The inset of (a) represents the plots for $R(t)$ vs. P_b at different time intervals indicated by various symbol types in the legends. (b) The effective growth exponent, ϕ_{eff} is plotted as a function of $1/t$ corresponding to the length scale presented in (a).

At much higher rates of bond-breaking probability, macrophase separation kinetics become completely dominant due to increased bond-degradation reactions. Consequently, the system behaves like an AB polymer blend, and the corresponding length scale transitions to the inertial hydrodynamic growth regime ($\phi \sim 2/3$) at late times. Hence, applying random photo-illumination at high-intensity results in a transition from microphase to macrophase separation kinetics for this system.

The inset of Fig. 3.10(a) depicts the $R(t)$ vs. P_b curves at different time intervals, as indicated in the legends. These curves demonstrate the power-law behavior of $R(t)$ over P_b given by $R(t) \sim a_0 + aP_b^{\nu}$. Here, a_0 represents the onset values of the length scale, which increase with time as follows: $a_0 = 4.2$, 4.5, 5.1, 5.4, and 5.6 for the black, red, green, blue, and magenta curves, respectively. Additionally, the parameters a and the power-law exponent ν also increase with time as follows: $a = 4.2$, 8.5, 11.1, 13.7, 16.3, and $\nu = 0.03$, 0.13, 0.17, 0.2, 0.23. Finally, in Fig. 3.10(b), we illustrate the effective growth exponent ϕ_{eff} against $1/t$ for different rates of bond-degradation reactions. As discussed earlier, the growth exponent decreases over time and tend towards zero for

$P_b = 0.01$ (cyan curve) and 0.1 (red curve). For $P_b = 0.2$, the increasing trend of the length scale begins at later times. For higher probabilities ($P_b > 0.2$), the values of ϕ_{eff} increase at later time intervals, indicating accelerated growth (see Fig. 3.10(a)). As $P_b \to 1.0$, $\phi_{eff} = 2/3$, representing inertial hydrodynamic growth at higher light intensities, characterizes macrophase separation kinetics. In summary, $P_b \sim 0.2$ can be considered the transition probability from microphase to macrophase length scale.

3.6 Summary and discussion

In this chapter, we studied the effect of random photo-illumination on the phase separation kinetics of polymer fluids using DPD technique. We explored the impact of photo-sensitive reactions on domain evolution, characterization functions, growth laws, and related parameters. We varied the bond-breaking probability $P_b \in (0, 1)$ (light on-state) to regulate the rate of bond-degradation reactions during light illumination, while the bond recombination probability was fixed at $P_c = 1.0$ during the off-state of the light.

We investigated the reaction kinetics from the plots of the cumulative number of bonds broken n_b against time and observed a power-law behavior: $n_b \sim t^\theta$ for different P_b values. Here, θ represents the power-law exponent. At lower bond-breaking probabilities, a linear behavior of n_b is noted with $\theta \sim 1.0$. However, the growth exponent decreases at higher probabilities ($P_b \to 1.0$), having values of $\theta \simeq 0.5$ for the polymer blend and $\theta \simeq 0.7$ for the BCP melt system at later times. The shift in RDF peaks towards higher r values represents domain coarsening over time for a fixed light intensity. However, for a fixed time interval, the primary peaks of RDF shift to the right at higher P_b values, indicating accelerated domain growth at higher light intensities. Correspondingly, the correlation function curves terminate at lower r/R values with increasing P_b. As P_b increases, the oscillatory nature of the correlation function diminishes, and the secondary hump of the

structure factor curves disappears, indicating the formation of a macrophase-separated structure at higher photo intensity.

From the characteristic length scale plots it is observed that, under random photo-illumination a transition from microphase to macrophase separation kinetics occurs over time. This outcome was noted in both systems. The length scale exhibits microphase separation behavior at early time intervals, following the diffusive growth regime ($\phi \sim 1/3$). However, the polymer blend system notes a slight deviation at higher P_b. As the intensity of light illumination increases, the growth scale transitions to the inertial hydrodynamic regime ($\phi \sim 2/3$) at late time intervals, indicating macrophase separation. From the plots of $R(t)$ vs. P_b and the effective growth exponent over time, we estimated the transition probabilities from microphase to macrophase separation kinetics as approximately $P_b \simeq 0.015$ for the polymer blend and $P_b \simeq 0.2$ for the BCP melt system. Thus, increasing the light intensity led to a crossover from micro to macrophase separation by applying random photo-illumination.

Given the significance of diverse morphologies arising from segregating polymer blends and block copolymer (BCP) melts, our objective is to establish a standardized framework for analyzing simulations and experiments involving externally responsive polymeric systems.